Atmos. Chem. Phys., 17, 6651–6662, 2017
https://doi.org/10.5194/acp-17-6651-2017

Atmospheric Chemistry and Physics
Open Access
EGU

A novel method for deriving the aerosol hygroscopicity parameter based only on measurements from a humidified nephelometer system

Ye Kuang[1], Chunsheng Zhao[1], Jiangchuan Tao[1], Yuxuan Bian[2], Nan Ma[3], and Gang Zhao[1]

[1]Department of Atmospheric and Oceanic Sciences, School of Physics, Peking University, Beijing, China
[2]State Key Laboratory of Severe Weather, Chinese Academy of Meteorological Sciences, Beijing, China
[3]Leibniz Institute for Tropospheric Research, Leipzig, Germany

Correspondence to: Chunsheng Zhao (zcs@pku.edu.cn)

Received: 29 November 2016 – Discussion started: 6 February 2017
Revised: 4 May 2017 – Accepted: 4 May 2017 – Published: 7 June 2017

Abstract. Aerosol hygroscopicity is crucial for understanding roles of aerosol particles in atmospheric chemistry and aerosol climate effects. Light-scattering enhancement factor $f(\mathrm{RH},\lambda)$ is one of the parameters describing aerosol hygroscopicity, which is defined as $f(\mathrm{RH},\lambda) = \sigma_{\mathrm{sp}}(\mathrm{RH},\lambda)/\sigma_{\mathrm{sp}}(\mathrm{dry},\lambda)$, where $\sigma_{\mathrm{sp}}(\mathrm{RH},\lambda)$ or $\sigma_{\mathrm{sp}}(\mathrm{dry},\lambda)$ represents σ_{sp} at wavelength λ under certain relative humidity (RH) or dry conditions. Traditionally, an overall hygroscopicity parameter κ can be retrieved from measured $f(\mathrm{RH},\lambda)$, hereinafter referred to as $\kappa_{f(\mathrm{RH})}$, by combining concurrently measured particle number size distribution (PNSD) and mass concentration of black carbon. In this paper, a new method is proposed to directly derive $\kappa_{f(\mathrm{RH})}$ based only on measurements from a three-wavelength humidified nephelometer system. The advantage of this newly proposed approach is that $\kappa_{f(\mathrm{RH})}$ can be estimated without any additional information about PNSD and black carbon. This method is verified with measurements from two different field campaigns. Values of $\kappa_{f(\mathrm{RH})}$ estimated from this new method agree very well with those retrieved by using the traditional method: all points lie near the 1 : 1 line and the square of correlation coefficient between them is 0.99. The verification results demonstrate that this newly proposed method of deriving $\kappa_{f(\mathrm{RH})}$ is applicable at different sites and in seasons of the North China Plain and might also be applicable in other regions around the world.

1 Introduction

Atmospheric aerosol particles play vital roles in visibility, energy balance, and the hydrological cycle of the Earth–atmosphere system and have attracted a lot of attention in recent decades. Aerosol particles suspended in the atmosphere directly influence radiative transfer of solar radiation and indirectly affect cloud properties and therefore have large impacts on climate change. In particular, uncertainties in direct aerosol radiative forcing due to anthropogenic aerosols and in aerosol indirect forcing caused by aerosol interaction with clouds contribute most to the total uncertainty in climate forcing (Boucher et al., 2013). One of the most important factors affecting these uncertainties is the interaction between aerosol particles and ambient atmospheric water vapor (Zhao et al., 2006; Kuang et al., 2016b). Under supersaturated conditions, aerosol particles serve as cloud condensation nuclei (CCN) and hence influence cloud properties. Under subsaturated conditions, with respect to typical aerosol compositions, water usually constitutes about half of the aerosol mass at a relative humidity (RH) of 80 % with substantially higher water mass fractions existing at RH values above 90 % for most ambient aerosol (Bian et al., 2014). The water content of aerosol and cloud droplets depends on both the ambient RH and hygroscopicity of the aerosol chemical constituents.

Traditionally, the Köhler theory (Petters and Kreidenweis, 2007) is widely used to describe the hygroscopic growth of aerosol particles and is successfully used in laboratory studies for single-component and some multicomponent particles. In order to account for the mixed organic and inor-

ganic composition of ambient aerosol, Petters and Kreidenweis (2007) proposed a modified version of the Köhler theory called the κ-Köhler theory to describe a single aerosol hygroscopic growth parameter, κ. The κ-Köhler equation, expressed in terms of the diameter growth factor, g(RH), is given in Eq. (1) below:

$$\frac{\mathrm{RH}}{100} = \frac{g^3 - 1}{g^3 - (1-\kappa)} \cdot \exp\left(\frac{4\sigma_{\mathrm{s/a}} \cdot M_{\mathrm{water}}}{R \cdot T \cdot D_{\mathrm{d}} \cdot g \cdot \rho_{\mathrm{w}}}\right), \quad (1)$$

where g corresponds to g(RH), D_{d} is the dry diameter, $\sigma_{\mathrm{s/a}}$ is the surface tension of the solution–air interface, T is the temperature, M_{water} is the molecular weight of water, R is the universal gas constant, ρ_{w} is the density of water, and κ is the hygroscopicity parameter. This theory is not only applicable to single-component aerosol particles, but also to multicomponent aerosol particles. With regard to a multicomponent aerosol particle, the Zdanovskii–Stokes–Robinson assumption can be applied. The hygroscopicity parameter κ of a multicomponent aerosol particle can be derived by using the following formula: $\kappa = \sum_i \varepsilon_i \cdot \kappa_i$, where κ_i and ε_i represent the hygroscopic parameter and volume fraction of each component. This hygroscopicity parameter κ has received much attentions and turns out to be a very effective parameter for studying aerosol hygroscopicity. The hygroscopicity parameter κ makes the comparison of the aerosol hygroscopicity at different sites around the world and different time periods more convenient. In addition, hygroscopicity parameter κ also facilitates the intercomparison of aerosol hygroscopicity derived from different techniques and measurements made at different RHs. The hygroscopicity parameter κ is widely used to account for the influence of aerosol hygroscopic growth on aerosol optical properties as well as aerosol liquid water contents (Tao et al., 2014; Kuang et al., 2015; Brock et al., 2016; Bian et al., 2014; Zieger et al., 2013) and to examine the role of aerosol hygroscopicity in CCN (Chen et al., 2014; Gunthe et al., 2009; Ervens et al., 2010). The κ values derived from field campaigns and laboratory studies will further our understanding of aerosol hygroscopicity and help estimate the influences of aerosol hygroscopic growth on different aspects of atmospheric processes.

The humidity tandem differential mobility analyzer (HTDMA) measures the aerosol diameter hygroscopic growth as a function of RH. The aerosol hygroscopicity parameter κ can be directly derived from measurements of HTDMA by applying Eq. (1) (Liu et al., 2011; Wu et al., 2016). HTDMA systems can provide insights into the aerosol hygroscopicity at different aerosol diameters. However, they can only be used to derive aerosol hygroscopicity parameter κ within a certain size range (usually less than 300 nm). HTDMA systems are not capable of providing more details about the hygroscopicity of aerosol particles that contribute most to aerosol optical properties and aerosol liquid water contents (their diameters usually ranging from 200 nm to 1 µm) (Ma et al., 2012; Bian et al., 2014). The effect of aerosol water uptake on the aerosol particle light scattering (σ_{sp}) is usually measured with a humidified nephelometer system. Measurements from a humidified nephelometer system can also be used to calculate the aerosol hygroscopicity parameter κ if the dry aerosol particle number size distribution (PNSD) is measured simultaneously (Chen et al., 2014). The scattering enhancement factor $f(\mathrm{RH}, \lambda)$, defined as $f(\mathrm{RH}, \lambda) = \sigma_{\mathrm{sp}}(\mathrm{RH}, \lambda)/\sigma_{\mathrm{sp}}(\mathrm{dry}, \lambda)$, characterizes changes in the aerosol scattering coefficient with RH. $\sigma_{\mathrm{sp}}(\mathrm{RH}\lambda)$ or $\sigma_{\mathrm{sp}}(\mathrm{dry}\lambda)$ represent σ_{sp} at wavelength λ at a certain RH or under dry conditions. In this research, f(RH) is referred to as $f(\mathrm{RH}, 550\,\mathrm{nm})$. The nephelometer measures aerosol optical properties of the entire aerosol size distribution. Thus, κ calculated from f(RH) measurements can be understood as an optically weighted κ and represents the overall hygroscopicity of ambient aerosol particles. This κ is more suitable for being used to account for the influences of aerosol hygroscopic growth on aerosol optical properties compared to aerosol hygroscopicity derived from HTDMA measurements. Traditionally, derivation of κ from f(RH) measurements requires aerosol PNSD as well as black carbon (BC) measurements to determine the imaginary part of the refractive index. As PNSD and BC measurements are expensive, their availability in field campaigns is limited.

In this paper we use measurements from a field campaign on the North China Plain (NCP) to derive κ values using three methods. The first two methods derive κ from aerosol diameter hygroscopic growth and the third method derives an aerosol optical parameterization of κ. Method 1, labeled as $\kappa_{f(\mathrm{RH})}$, derives κ from aerosol PNSD, BC, and nephelometer f(RH) measurements. Method 2, defined as κ_{250}, derives κ from g(RH) measurements of aerosol particles with a diameter of 250 nm, using a high-humidity tandem differential mobility analyzer (HH-TDMA). HH-TDMA is a system very similar to HTDMA but is capable of operating at higher RH points (Liu et al., 2011). Method 3, defined as κ_{sca}, is an empirical determination of κ using only nephelometer measurements of the aerosol scattering coefficient as a function of RH.

Based on detailed analysis of the relationship between $\kappa_{f(\mathrm{RH})}$ and κ_{sca}, a novel method for directly deriving $\kappa_{f(\mathrm{RH})}$ based only on measurements from a humidified nephelometer system is proposed. This newly proposed approach makes it more convenient and cheaper for researchers to conduct aerosol hygroscopicity research with f(RH) measurements.

2 Site description and instruments

Datasets from five field campaigns are used in this paper. The five campaigns are conducted at four different measurement sites of the NCP (Wangdu, Xianghe, and Gucheng in Hebei province and Wuqing in Tianjin; site locations are shown in Fig. S1 in the Supplement). Time periods and datasets from these filed campaigns that were used are listed in Table 1.

Table 1. Locations, time periods, and datasets of five field campaigns that were used.

Location	Wuqing	Wuqing	Xianghe	Wangdu	Gucheng
Time period	7 Mar to 4 Apr 2009	12 Jul to 14 Aug 2009	9 Jul to 8 Aug 2013	4 Jun to 14 Jul 2014	15 Oct to 25 Nov 2016
PNSD	TSMPS + APS	TSMPS + APS	TSMPS + APS	TSMPS + APS	SMPS + APS
BC	MAAP	MAAP	MAAP	MAAP	AE33
σ_{sp}	TSI 3563	TSI 3563	TSI 3563	TSI 3563	Aurora 3000
$f(RH)$				Humidified nephelometer system	Humidified nephelometer system
$g(RH)$				HH-TDMA	

During these field campaigns, sampled aerosol particles have aerodynamic diameters less than 10 µm (selected by passing through an impactor). Aerosol PNSDs with a particle diameter ranging from 3 nm to 10 µm were jointly measured by a twin differential mobility particle sizer (TDMPS, Leibniz Institute for Tropospheric Research (IfT), Germany; Birmili et al., 1999) or a scanning mobility particle size spectrometer (SMPS) and an aerodynamic particle sizer (APS, TSI Inc., model 3321) with a temporal resolution of 10 min. The mass concentrations of BC were measured using a multi-angle absorption photometer (MAAP model 5012, Thermo, Inc., Waltham, MA USA) or an Aethalometer called AE33 (Drinovec et al., 2015). The aerosol light-scattering coefficients (σ_{sp}) at three wavelengths were measured using a TSI 3563 nephelometer (Anderson and Ogren, 1998) or an Aurora 3000 nephelometer (Müller et al., 2011).

A humidified nephelometer system consists of two nephelometers, and a humidifier was used in the Wangdu and Gucheng campaigns. For the humidified nephelometer systems that we have designed, they only scan the hydration branch of the aerosol hygroscopic growth. The humidifier humidified the sample air through a Gore-Tex tube. The water vapor penetrates through the Gore-Tex tube, which is surrounded by a circulating water layer in a stainless steel tube. The temperature cycle of the circulating water layer was specified and controlled by a water bath. During the Wangdu campaign, only one water bath was used. For each RH scanning cycle, the temperature cycle was fixed. Thus, the RH range of each cycle will change. Since the room temperature of the container was relatively stable during the Wangdu campaign, the RH points of $f(RH)$ cycles range from about 50 % to about 90 %, and each cycle lasted about 45 min. However, one cycle cost about 90 min because after each cycle was finished, the water bath needed about another 45 min to cool. During the Gucheng campaign, this problem is solved by using two water baths and they provided circulating water alternatively for the humidifier. The corresponding temporal resolution of $f(RH)$ cycles was about 45 min. In addition, a control software system was developed and could make sure the RH scans were within a certain RH range. During the Gucheng campaign, the RH points of each $f(RH)$ cycle range from 45 to 90 %. During the Wangdu campaign, the two nephelometers operated in series, and a TSI 3563 nephelometer was used. During the Gucheng campaign, the two nephelometers operated in parallel, and Aurora 3000 nephelometers were used. In the following, we refer to the nephelometer that measures σ_{sp} in a dry state and the nephelometer that measures σ_{sp} at different RH points as dry Neph and wet Neph, respectively. Two combined RH and temperature sensors (Vaisala HMP110; accuracy of $\pm 0.2°$ and ± 1.7 % for RH ranges from 0 to 90 %, respectively, and accuracy of ± 2.5 % for RH ranges from 90 to 100 % according to the manufacturer) are placed at the inlet and outlet of the wet Neph, and the measured RHs and temperatures are defined as RH_1/T_1 and RH_2/T_2, respectively. The dew points at the inlet and outlet of wet Neph were calculated using the measured RH_1/T_1 and RH_2/T_2, and the average value was considered as the dew point of the sample air. The sample RH can be calculated through the derived dew point and the sample temperature, which is measured by the sensor inside the sample cavity of the nephelometer. During the Wangdu campaign, measurements from the humidified nephelometer system were only available from 21 June 2014 to 1 July 2014. During the two campaigns, the two nephelometers were calibrated every 2 weeks. The manufacturer of HMP110 suggests that the sensors should be calibrated yearly. We did not calibrate the HMP110 sensors that were used during the two campaigns because they had only been used less than 3 months, and results of cross checks showed that they agree well with each other. The sample RHs in the dry Neph were about 20 % and about 8 % during the Wangdu and Gucheng campaigns, respectively.

The dataset includes aerosol PNSDs at dry state and mass concentrations of BC. σ_{sp} values of different wavelengths from the following four campaigns, which are listed in Table 1, are referred to as dataset D1: the two campaigns conducted in Wuqing, the Xianghe campaign, and the Wangdu campaign before 21 June 2014. Note that measured σ_{sp} values of dataset D1 are not corrected for angular truncation errors. This is because dataset D1 is used for producing the look-up table of the newly proposed method, and it is expected that the Ångström exponent calculated from measured σ_{sp} values can be directly used as input for the newly proposed method. However, for σ_{sp} values shown in Fig. 1, the angular truncation errors are corrected using the Mie theory with measured PNSD and mass concentrations of BC.

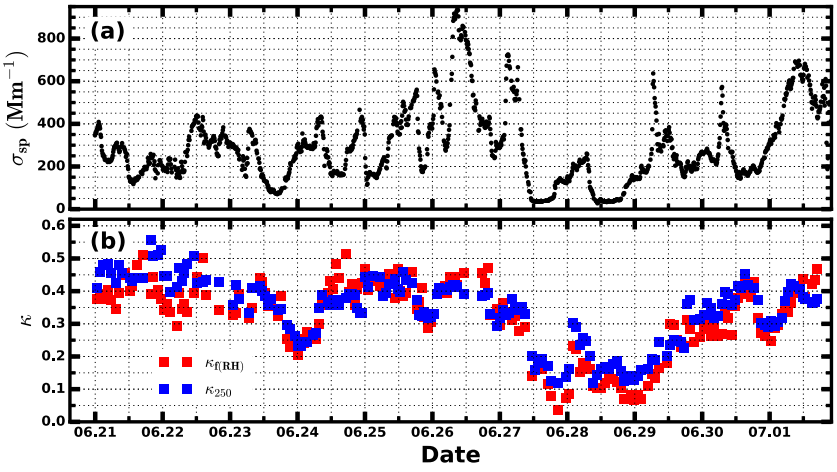

Figure 1. **(a)** The time series of σ_{sp} at 550 nm. **(b)** The time series of κ values derived from f(RH) measurements ($\kappa_{f(RH)}$) by combining information on PNSD and BC, and time series of average κ values of aerosol particles at 250 nm (κ_{250}), which are calculated from measurements of HH-TDMA.

During the Wangdu campaign, the growth factors of aerosol particles at six selected particle diameters (30, 50, 100, 150, 200, and 250 nm) at 98 % RH were obtained from the measurements of the HH-TDMA (IfT, Germany; Hennig et al., 2005). For detailed information about HH-TDMA measurements, please refer to Liu et al. (2011)

3 Methodology

3.1 Calculations of hygroscopicity parameter κ from f(RH) measurements

Research of Chen et al. (2014) demonstrated that if the PNSD at dry state is measured, then measurements of f(RH) can be used to derive the aerosol hygroscopicity parameter κ by conducting an iterative calculation with the Mie theory and the κ-Köhler theory. To reduce the influence of random errors of observed f(RH) at a certain RH, all valid f(RH) measurements in a complete humidifying cycle are used in the derivation algorithm. The retrieved κ is the κ value that can be used to best fit the observed f(RH) curve, labeled as $\kappa_{f(RH)}$, and this method of deriving κ is Method 1. Details about this retrieval algorithm are described in Chen et al. (2014). Of particular note is that in this research the mass concentration of BC is also considered in the retrieval algorithm to account for the influence of BC on refractive indices of aerosol particles at different sizes. During the simulation process, aerosol components are divided into two classes in terms of their optical properties: the light absorbing component (i.e., BC) and less absorbent components (comprising inorganic salts and acids such as sulfates, nitrates, ammonium, and most organic compounds). BC is considered to be homogeneously mixed with other aerosol components, and the mass size distribution of BC used in Ma et al. (2012), which is observed on the NCP, is used in this research to account for the mass distributions of BC at different particle sizes. The refractive index and density of BC that were used are $1.80 - 0.54\,i$ and $1.5\,\mathrm{g\,cm^{-3}}$ (Kuang et al., 2015). The refractive indices of non-light-absorbing aerosol components (other than BC) and liquid water that were used are $1.53 - 10^{-7}\,i$ (Wex et al., 2002) and $1.33 - 10^{-7}\,i$ (Seinfeld and Pandis, 2006), respectively. The flow chart about this retrieval algorithm is also introduced in the Supplement. Please refer to Fig. S2 for more details.

3.2 Calculations of hygroscopicity parameter κ from HH-TDMA measurements

The HH-TDMA measures geometric hygroscopic growth factors of particles at different sizes at 98 % RH. The measured hygroscopic factors can be directly related to κ with Eq. (1). For a specified size of selected aerosol particles, a distribution of growth factors can be measured, and thus can be used to derive a probability distribution of κ and finally come to the calculation of an average κ value corresponding to this size of aerosol particles. The method for deriving average κ value of a certain size of aerosol particles from HH-TDMA measurements is elaborately described in Liu et al. (2011). In this research κ values derived from g(RH) measurements of aerosol particles with a diameter of 250 nm are used, defined as κ_{250}. This method of deriving κ is Method 2.

3.3 Parameterization schemes for f(RH)

The most frequently used f(RH) parameterization scheme is a power-law function that is known as gamma parameterization (Titos et al., 2016) and the formula of this single-

parameter representation is written as the following:

$$f(\mathrm{RH}) = \left[\frac{100-\mathrm{RH}_0}{100-\mathrm{RH}}\right]^{\gamma}, \quad (2)$$

where RH_0 is the RH of the dry condition, and γ is a parameter fitted to the observed $f(\mathrm{RH})$. In this study, we estimated γ values with observed $f(\mathrm{RH})$ curves and to our knowledge, we are the first ones to further examine the relationship between γ and $\kappa_{f(\mathrm{RH})}$.

Recently, a new physically based single-parameter representation was proposed by Brock et al. (2016) to describe $f(\mathrm{RH})$. Their results demonstrated that this proposed parameterization scheme can better describe $f(\mathrm{RH})$ than the widely used gamma power-law approximation (Brock et al., 2016). The formula of this new scheme is written as

$$f(\mathrm{RH}) = 1 + \kappa_{\mathrm{sca}}\frac{\mathrm{RH}}{100-\mathrm{RH}}, \quad (3)$$

where κ_{sca} is a parameter that fits $f(\mathrm{RH})$ best. Regardless of the curvature effects for particle diameters larger than 100 nm, the hygroscopic growth factor for aerosol particles can be approximately expressed as the following (Brock et al., 2016): $g\,f_{\mathrm{diam}} \cong (1+\kappa\frac{\mathrm{RH}}{100-\mathrm{RH}})^{1/3}$. Moreover, σ_{sp} is usually approximately proportional to total aerosol volume (Pinnick et al., 1980), which means that the relative change in σ_{sp} due to aerosol water uptake is roughly proportional to the relative change in aerosol volume. The enhancement factor in volume can be expressed as the cube of $g\,f_{\mathrm{diam}}$, thus leading to the formula form of $f(\mathrm{RH})$ expressed in Eq. (3).

During processes of measuring $f(\mathrm{RH})$, the sample RH in the dry Neph condition (RH_0) is not zero. According to Eq. (3), the measured $f(\mathrm{RH})_{\mathrm{measure}} = \frac{f(\mathrm{RH})}{f(\mathrm{RH}_0)}$ should be fitted using the following formula:

$$f(\mathrm{RH})_{\mathrm{measure}} = \frac{1+\kappa_{\mathrm{sca}}\frac{\mathrm{RH}}{100-\mathrm{RH}}}{1+\kappa_{\mathrm{sca}}\frac{\mathrm{RH}_0}{100-\mathrm{RH}_0}}. \quad (4)$$

The method of calculating κ_{sca} by curve fitting using Eq. (4) is called Method 3. The gamma parameterization scheme is referred to as γ Method in the following paragraphs.

4 Results and discussions

4.1 κ values derived from $f(\mathrm{RH})$ and HH-TDMA measurements

During this field campaign, the aerosol physical, chemical, and optical properties were synergistically observed with different types of instruments. They provide valuable datasets to perform an insightful analysis on aerosol hygroscopicity and its relationship with other aerosol properties. The time series of σ_{sp} at 550 nm in a dry state are shown in Fig. 1a. The results show that this observation period has experienced varying degrees of pollution levels, with σ_{sp} at 550 nm ranging from 15 to 1150 $\mathrm{M\,m^{-1}}$. Values of $\kappa_{f(\mathrm{RH})}$ derived from Method 1 are shown in Fig. 1b. During deliquescence $f(\mathrm{RH})$ exhibits an abrupt increase between RH values of 60–65 %. As such, only $f(\mathrm{RH})$ data points with RH > 70 % were used in determination of $\kappa_{f(\mathrm{RH})}$ when deliquescence was apparent. For $f(\mathrm{RH})$ cycles without deliquescence, all $f(\mathrm{RH})$ points are used in the retrieval algorithm with RH ranges of about 50 to 90 %. The results demonstrate that $\kappa_{f(\mathrm{RH})}$ lies between 0.06 and 0.51, with an average of 0.32. The lowest $\kappa_{f(\mathrm{RH})}$ values are found when the air quality is relatively clean (σ_{sp} at 550 nm is lower than 100 $\mathrm{M\,m^{-1}}$) on 27 and 28 June. During these 2 days, organic matter dominates the mass concentration of $\mathrm{PM}_{2.5}$, which results in the low hygroscopicity of aerosol particles (Kuang et al., 2016a). Conversely, the largest $\kappa_{f(\mathrm{RH})}$ values are found during periods when deliquescent phenomena occur and inorganic chemical compositions dominate the mass concentrations of $\mathrm{PM}_{2.5}$; sulfate is especially highly abundant during these periods. Of particular note is that during relatively polluted periods (σ_{sp} at 550 nm larger than 100 $\mathrm{M\,m^{-1}}$) aerosol particles are generally very hygroscopic, which implies that aerosol water uptake can exert significant impacts on regional direct aerosol radiative effect and ambient visibility during this observation period.

On the basis of the average size-resolved κ distribution from the Haze in China (HaChi) campaign (Liu et al., 2014), κ values change a lot for aerosol particles whose diameters are less than 250 nm; however, κ values vary relatively less for aerosol particles whose diameters range from 250 nm to 1 µm. In addition, the results from the HaChi campaign also demonstrate that aerosol particles whose diameters range from 200 nm to 1 µm usually contribute more than 80 % to σ_{sp} at 550 nm during summer on the NCP (Ma et al., 2012). That is, $\kappa_{f(\mathrm{RH})}$ may share a similar magnitude with κ_{250}. To compare κ values derived from Method 1 and Method 2, values of κ_{250} are also shown in Fig. 1b. During this observation period, values of κ_{250} range from 0.11 to 0.56, with an average of 0.34, which is very close to average κ_{250} observed during the HaChi campaign (Liu et al., 2011). The results shown in Fig. 1b suggest that, in general, $\kappa_{f(\mathrm{RH})}$ values agree well with κ_{250} values. However, they are usually lower than κ_{250} values. To quantitatively compare these two types of κ values, they are plotted against each other and shown in Fig. 2. It can be seen that they are highly correlated, but overall the κ_{250} values are higher than $\kappa_{f(\mathrm{RH})}$ values, and the average difference between κ_{250} and $\kappa_{f(\mathrm{RH})}$ is 0.02. The statistical relationship between κ_{250} and $\kappa_{f(\mathrm{RH})}$ is also shown in Fig. 2. This relationship may be useful for researchers if they want to estimate the influences of aerosol water uptake on aerosol optical properties and aerosol liquid water contents when only HH-TDMA or HTDMA measurements are available.

A model experiment is conducted to better understand the relationship between κ_{250} and $\kappa_{f(\mathrm{RH})}$. During the HaChi campaign, size-resolved κ distributions are derived from

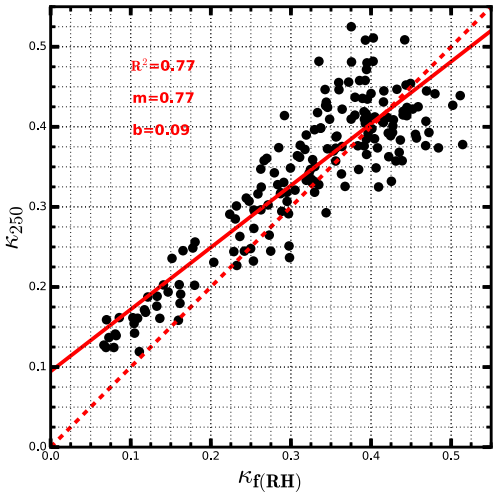

Figure 2. The comparison between κ values derived from $f(\mathrm{RH})$ measurements ($\kappa_{f(\mathrm{RH})}$) and average κ values for aerosol particles with a diameter of 250 nm (κ_{250}), which are derived from measurements of HH-TDMA. R^2 is the square of the correlation coefficient, m is the slope, and b is the intercept.

measured size-segregated chemical compositions (Liu et al., 2014) and their average is used in this experiment to account for the size dependence of aerosol hygroscopicity, which is shown in Fig. 3a. With this average size-resolved κ distribution, all observed PNSDs in a dry state along with mass concentrations of BC from dataset D1 are used to simulate the retrieval of $\kappa_{f(\mathrm{RH})}$ under different PNSD and BC conditions. The PNSDs that were used, shown in Fig. 3b, indicate that large varying types of PNSDs are considered in the simulative experiment. As for the simulation process, with given PNSD, mass concentration of BC and size-resolved κ distribution, two steps are required. The first step is simulating $f(\mathrm{RH})$ points using the Mie theory and the κ-Köhler theory with RH range of 50 to 90 % and a RH interval of 10 %. The second step is retrieving corresponding $\kappa_{f(\mathrm{RH})}$ using the procedure of Method 1. The κ value at a particle diameter of 250 nm of the size-resolved κ distribution that was used is the corresponding κ_{250}. The probability distribution of simulated $\kappa_{f(\mathrm{RH})}$ is also shown in Fig. 3a. The standard deviation of retrieved $\kappa_{f(\mathrm{RH})}$ is about 0.01, which suggests that if the size-resolved κ distribution is fixed, then $\kappa_{f(\mathrm{RH})}$ varies little. Because $\kappa_{f(\mathrm{RH})}$ represents an overall, size-integrated κ, it is clearly shown in Fig. 3a that in most cases $\kappa_{f(\mathrm{RH})}$ values are within κ values of aerosol particles ranging from 200 nm to 1 µm. Moreover, about 70 % of simulated $\kappa_{f(\mathrm{RH})}$ values are less than κ_{250}, which to some extent explains the observed difference between κ_{250} and $\kappa_{f(\mathrm{RH})}$ mentioned before. However, the simulated average difference between κ_{250} and average $\kappa_{f(\mathrm{RH})}$ is about 0.01 which is less than the observed averaged difference between κ_{250} and $\kappa_{f(\mathrm{RH})}$, which is 0.02. In particular, when $\kappa_{f(\mathrm{RH})}$ values are relatively lower (< 0.25), the κ_{250} is systematically higher than $\kappa_{f(\mathrm{RH})}$. Except for uncertainties from measurements of instruments, for example, the uncertainty of RH in measurements of HH-TDMA and uncertainties of measuring $f(\mathrm{RH})$ (details about the uncertainty sources of $f(\mathrm{RH})$ measurements can be found in the paper published by Titos et al., 2016), there are two other reasons that may be associated with the discrepancy between κ_{250} and $\kappa_{f(\mathrm{RH})}$. The first reason is that configurations of size-resolved κ distributions and PNSDs during this field campaign are far different from the model experiment. The second reason is that in the real atmosphere, κ values at different RH conditions may be different (You et al., 2014) and most $f(\mathrm{RH})$ measurements are conducted when RH is lower than 90 %. However, the measurements of HH-TDMA are conducted when RH is equal to 98 %. Overall, the observed general consistency between κ values derived from measurements of $f(\mathrm{RH})$ and HH-TDMA confirms the reliability of κ values derived from $f(\mathrm{RH})$ measurements.

4.2 Relationships between κ derived from $f(\mathrm{RH})$ measurements and $f(\mathrm{RH})$ fitting parameters

In the previous section, derived $\kappa_{f(\mathrm{RH})}$ values are characterized and compared with κ_{250} values. These results demonstrated that derived $\kappa_{f(\mathrm{RH})}$ values can commendably represent variations in aerosol hygroscopicity of ambient aerosol populations. In this section, the relationship between derived $\kappa_{f(\mathrm{RH})}$ values and $f(\mathrm{RH})$ fitting parameters is further examined to investigate their relationships.

Two parameterization schemes of $f(\mathrm{RH})$ are discussed in this paper, including the γ Method and Method 3. Values of γ and κ_{sca} are fitted from observed $f(\mathrm{RH})$ cycles during the Wangdu campaign. For cycles during deliquescent periods, only $f(\mathrm{RH})$ points with a RH higher than 70 % are used to perform fitting processes. The relationship between $\kappa_{f(\mathrm{RH})}$ and γ is investigated and shown in Fig. 4a. It is found that an approximately linear relationship exists (square of correlation coefficient is 0.90) between $\kappa_{f(\mathrm{RH})}$ and γ, especially when $\kappa_{f(\mathrm{RH})}$ is larger than 0.2. Fitted γ ranges from 0.13 to 0.56 with an average of 0.41.

During the Wangdu campaign, fitted κ_{sca} ranges from 0.05 to 0.36 with an average of 0.22. The relationship between $\kappa_{f(\mathrm{RH})}$ and κ_{sca} is also investigated and shown in Fig. 4b. It is found that a strong linear relationship also exists (square of correlation coefficient is 0.97) between $\kappa_{f(\mathrm{RH})}$ and κ_{sca}. The statistically fitted line almost passes though the zero point, which implies that a proportional relationship may exist between $\kappa_{f(\mathrm{RH})}$ and κ_{sca}. This strong correlation should be intrinsic due to Method 3 based on the fact that σ_{sp} is roughly proportional to total aerosol volume, and the volume growth factor is directly linked to the overall aerosol hygroscopicity parameter κ due to aerosol water uptake as discussed in Sect. 3.3. It seems that this promising linear relationship can help bridge the gap between $f(\mathrm{RH})$ and κ. However, results from Brock et al. (2016) imply that the relationship between $\kappa_{f(\mathrm{RH})}$ and κ_{sca} is much more sophisticated and it is affected

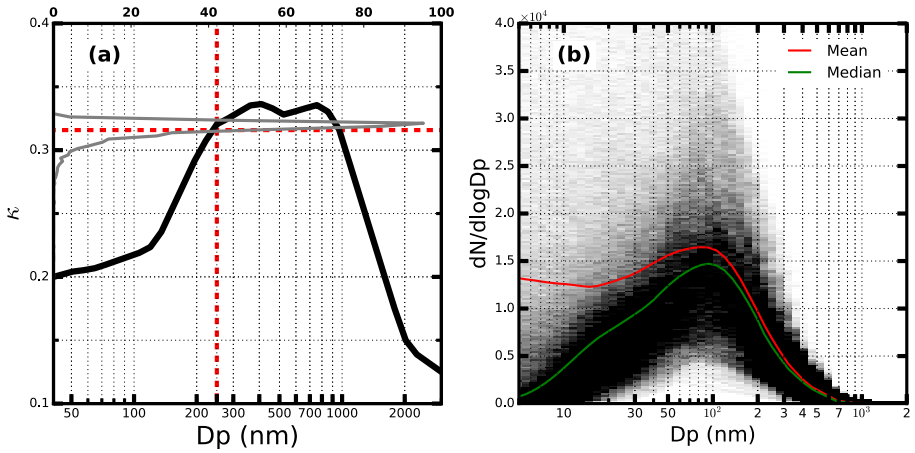

Figure 3. (a) The thick black line represents the average size-resolved κ distribution from the HaChi campaign. The solid gray line represents the probability distribution of retrieved κ values with this size-resolved κ distribution by using all PNSDs shown in **(b)**, and the horizontal dashed line represents their average. The vertical dashed red line represents the position of 250 nm. **(b)** All PNSDs that are observed from three different representative background sites of the NCP during summer; they are used to model the relationship between size-resolved κ and retrieved κ values from f(RH) measurements, and the gray color represents the frequency of PNSD. Darker points correspond to a higher frequency. The red and green lines represent the mean of median values of all observed PNSDs.

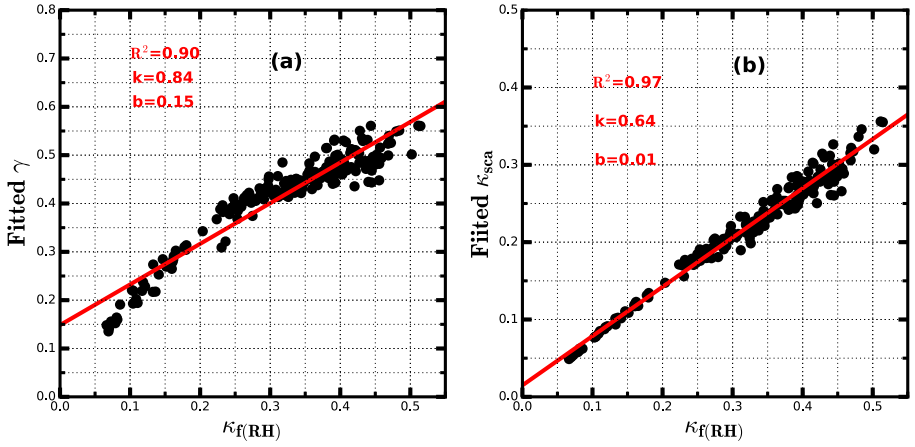

Figure 4. (a) The linear relationship between values of $\kappa_{f(\mathrm{RH})}$ and fitted γ. R^2 is the square of correlation coefficient, k is the slope, and b is the intercept. **(b)** The linear relationship between values of $\kappa_{f(\mathrm{RH})}$ and fitted κ_{sca}.

by both aerosol hygroscopicity and PNSD in a dry state. In the paper published by Brock et al. (2016), κ_{ext} (a parameter determined from measurements of the aerosol extinction coefficient as a function of RH using the formula form of Eq. 2) and κ_{chem} (a constant κ determined from chemical constituents of the entire aerosol population) are used and correspond to κ_{sca} and $\kappa_{f(\mathrm{RH})}$ in this research. The difference between κ_{ext} and κ_{sca} is that κ_{ext} is used to fit the light enhancement factor of the aerosol extinction coefficient, κ_{chem} and $\kappa_{f(\mathrm{RH})}$ actually mean the same because both of them are overall and size-independent hygroscopicity parameters. Results from Brock et al. (2016) concluded that the ratio $\kappa_{\mathrm{ext}}/\kappa_{\mathrm{chem}}$ generally lies between 0.6 and 1, which implies that the ratio $\kappa_{\mathrm{sca}}/\kappa_{f(\mathrm{RH})}$ (in the following, this ratio is referred to as R_κ) should also have large variations and may share a similar range of variability. By revisiting the relationship between $\kappa_{f(\mathrm{RH})}$ and κ_{sca} found in this research, it can be found that R_κ during this field campaign ranges from 0.58 to 0.77, with an average of 0.69. This result suggests that directly establishing a linkage between $\kappa_{f(\mathrm{RH})}$ and κ_{sca} with an average R_κ can result in a non-negligible bias (relative difference can reach about 15 %). In addition, this range of R_κ only represents the relationship between $\kappa_{f(\mathrm{RH})}$ and κ_{sca} during a short time period and at only one site.

To better understand the relationship between $\kappa_{f(\mathrm{RH})}$ and κ_{sca}, all PNSDs in a dry state (shown in Fig. 3a) along with mass concentrations of BC from dataset D1 are used to simulate the relationship between $\kappa_{f(\mathrm{RH})}$ and κ_{sca} with the Mie

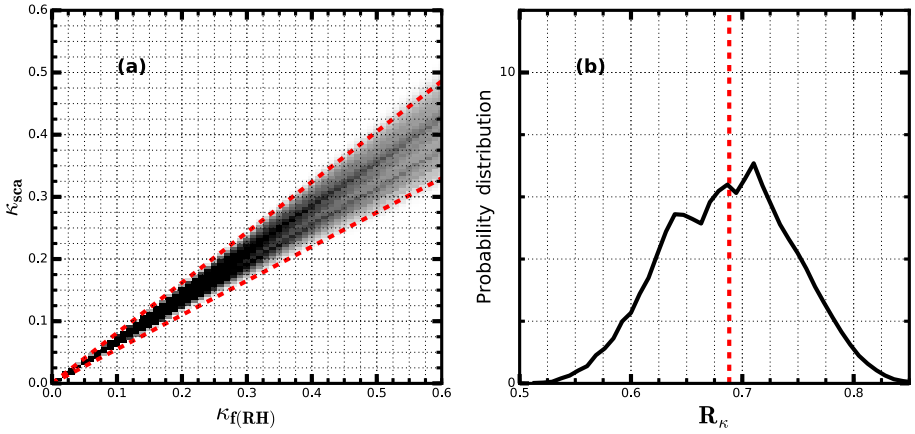

Figure 5. (a) Simulated relationships between $\kappa_{f(\mathrm{RH})}$ and κ_{sca} under different PNSD conditions (all PNSDs shown in Fig. 3a are used as inputs to conduct the simulation experiment). The gray color represents the frequency and darker points correspond to a higher frequency. The slopes of the two dashed lines are 0.55 and 0.81. **(b)** The probability distribution of R_κ ($\kappa_{\mathrm{sca}}/\kappa_{f(\mathrm{RH})}$).

and κ-Köhler theories. The aim of including PNSD and BC information from different campaigns is to simulate variations in R_k under different conditions. During simulation processes, for each PNSD we change $\kappa_{f(\mathrm{RH})}$ from 0.01 to 0.7 with an interval of 0.01 to examine the influence of aerosol hygroscopicity on R_κ. For each PNSD and $\kappa_{f(\mathrm{RH})}$, the simulation processes include two steps. The first step is simulating $f(\mathrm{RH})$ points using the Mie theory and the κ-Köhler theory with a RH range of 50 to 90 % and a RH interval of 10 %. The way of treating BC is the same as the retrieval procedure of $\kappa_{f(\mathrm{RH})}$ introduced in Sect.3.1. The second step is retrieving the corresponding $\kappa_{f(\mathrm{RH})}$ using the procedure of Method 1 and calculating κ_{sca} with Method 3. Simulated results of $\kappa_{f(\mathrm{RH})}$ and κ_{sca} are shown in Fig. 5a and the probability distribution of corresponding R_κ values is shown in Fig. 5b. The results show that R_κ primarily ranges from 0.5 to 0.84 with an average of 0.69, which is the same as the average R_κ measured during the Wangdu campaign. These results also indicate that the relationship between $\kappa_{f(\mathrm{RH})}$ and κ_{sca} is much more complex than a simple linear relationship and more information about aerosol properties are necessary to gain insights into the variation in R_κ.

4.3 A novel method for directly deriving κ from measurements of a humidified nephelometer system

A robust linear relationship is found between $\kappa_{f(\mathrm{RH})}$ and κ_{sca} in Sect. 4.2. However, results of further analysis suggest that R_κ varies a lot. The complexity comes from both PNSD in a dry state and aerosol hygroscopicity having impacts on R_κ. Generally, the nephelometers used in a humidified nephelometer system have three wavelengths (Titos et al., 2016) and the spectral dependence of σ_{sp} is usually described by the following Ångström formula: $\sigma_{\mathrm{sp}}(\lambda) = \beta\lambda^{-\alpha_{\mathrm{sp}}}$, where β is the particle number concentration dependent coefficient, λ is the wavelength of light, and α_{sp} represents the Ångström exponent of σ_{sp}. The Ångström exponent can be directly inferred from the measurements of σ_{sp} at different wavelengths. Of particular note is that the Ångström exponent can not only be used to account for the spectral course of σ_{sp} but it also reveals information about PNSD. In general, a larger value of the Ångström exponent corresponds to smaller aerosol particles. That is, the Ångström exponent can be a proxy of PNSD in a dry state and be used in the processes of estimating the impacts of PNSD on R_κ. Conversely, with regard to aerosol hygroscopicity, although R_κ varies within a certain range, the value of κ_{sca} can still be used to represent the overall hygroscopicity of aerosol particles.

Simulated R_κ values introduced in the last paragraph of Sect.4.2 are spread into a two-dimensional gridded plot. They are simulated from all observed PNSDs and mass concentrations of BC in dataset D1. The first dimension is the Ångström exponent with an interval of 0.02 and the second dimension is κ_{sca} with an interval of 0.01. Average R_κ value within each grid is represented by color and shown in Fig. 6a. Values of Ångström exponents corresponding to different PNSDs are calculated from concurrently measured σ_{sp} values at 450 and 550 nm from the TSI 3563 nephelometer. Based on results shown in Fig. 6a, the different impacts of aerosol hygroscopicity and dry-scattering the Ångström exponent on R_κ can be distinguished to some extent. The results demonstrate that PNSD in a dry state play a more important role in the variations in R_κ than overall aerosol hygroscopicity. Overall, a larger value of the Ångström exponent corresponds to higher R_κ. Aerosol hygroscopicity exhibits different influences on R_κ when Ångström exponent values are different. On average, higher κ_{sca} corresponds to lower R_κ if the Ångström exponent is smaller than about 0.8, and higher κ_{sca} corresponds to higher R_κ if the Ångström ex-

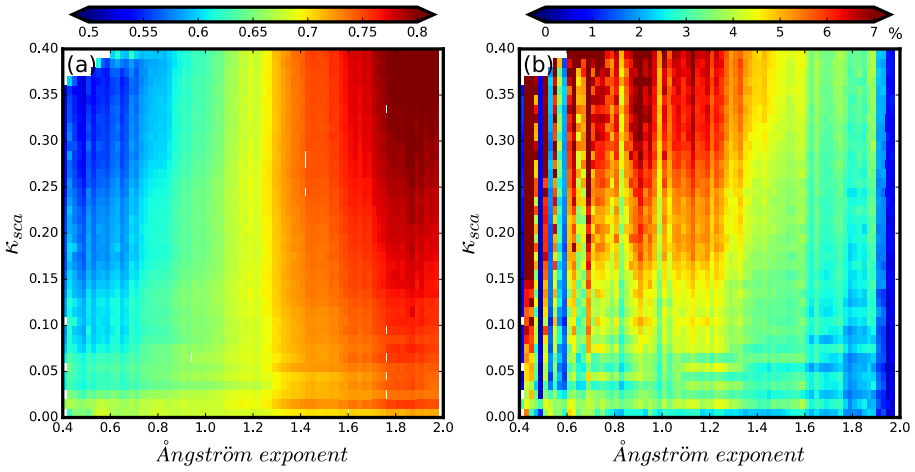

Figure 6. (a) Colors represent R_κ values and the color bar is shown at the top of this figure. The x axis represents the Ångström exponent and the y axis represents κ_{sca}. **(b)** Meanings of x axis and y axis are the same as in **(a)**; however, color represents the percentile value of the standard deviation of R_κ values within each grid divided by their average.

ponent is larger than about 1.6. The percentile value of the standard deviation of R_κ values within each grid of Fig. 6a divided by their average is shown in Fig. 6b. The Ångström exponent only represents an overall size property of aerosol particles. The same Ångström exponent corresponds to different aerosol PNSDs. Within each grid of Fig. 6a, the same κ_{sca} corresponds to different combinations of aerosol PNSD and $\kappa_{f(\mathrm{RH})}$, and R_κ values also change. Note that the size-dependent chemical composition also exerts influence on R_k. However, if PNSD is fixed, each size-resolved κ distribution corresponds to a certain $\kappa_{f(\mathrm{RH})}$, and $\kappa_{f(\mathrm{RH})}$ varies with a certain range no matter how size-resolved κ distribution changes. Therefore, influences of size-dependent chemical compositions on R_k are already included in the simulated results of producing the look-up table by varying the $\kappa_{f(\mathrm{RH})}$ from 0 to 0.7 for a fixed aerosol PNSD.

As shown in Fig. 6b, in most cases, these percentile values are less than 6 % (about 80 %), which demonstrates that R_κ varies little within each grid shown in Fig. 6a. This implies that results of Fig. 6a can be used as a look-up table to estimate R_κ. As mentioned before, the currently used nephelometer of a humidified nephelometer system usually has three wavelengths (Titos et al., 2016); thus, it can provide information about the Ångström exponent, and κ_{sca} can be directly fitted from the observed $f(\mathrm{RH})$ curve. Even if only one $f(\mathrm{RH})$ point is measured, κ_{sca} can still be calculated from Eq. (4). Using results shown in Fig. 6a as a look-up table, R_κ values can be directly predicted from measurements of a humidified nephelometer system. With this method, R_κ values during this Wangdu field campaign are predicted (values of the Ångström exponent are calculated from measured σ_{sp} values at 450 and 550 nm under dry conditions) and compared with measured R_κ values; the results are shown in Fig. 7a. The Ångström exponent during this field campaign ranges from 0.63 to 1.96, with an average of 1.4. It can be seen from Fig. 7a that the majority of points lie near the 1 : 1 line and 82 % of points have relative differences less than 6 %, which is consistent with results shown in Fig. 6b. This result is quite promising and can be further used to derive $\kappa_{f(\mathrm{RH})}$ values by combining fitted κ_{sca} and predicted R_κ. This method of deriving $\kappa_{f(\mathrm{RH})}$ is called Method 4 and includes two steps. The first step is calculating the Ångström exponent based on σ_{sp} values at 450 and 550 nm measured by the dry nephelometer and calculating κ_{sca} based on the $f(\mathrm{RH})$ curve measured by the humidified nephelometer system. The second step is predicting R_κ using the look-up table shown in Fig. 6a and then calculating $\kappa_{f(\mathrm{RH})}$ based on predicted R_κ and fitted κ_{sca}. The results of predicted $\kappa_{f(\mathrm{RH})}$ values are shown in Fig. 7b and a robust correlation between $\kappa_{f(\mathrm{RH})}$ values predicted from Method 4 and $\kappa_{f(\mathrm{RH})}$ values derived from Method 1 is achieved (the square of the correlation coefficient between them is 0.99). All points shown in Fig. 7b lie near the 1 : 1 line. The average difference between $\kappa_{f(\mathrm{RH})}$ is derived from Method 4 and Method 1 is -0.009.

Datasets from the Gucheng campaign are further used to verify Method 4. In this campaign, an Aurora 3000 nephelometer is used for the humidified nephelometer system, and it has three wavelengths: 450, 525, and 635 nm. Values of $f(\mathrm{RH}, \lambda)$ points correspond to wavelength of 525 nm are used to derive $\kappa_{f(\mathrm{RH})}$ using Method 1 and Method 4. The RH ranges from 45 to 90 %. The look-up table shown in Fig. 6a is simulated corresponding to a scattering wavelength of 550 nm and is not suitable for being used in Method 4 if the nephelometer is an Aurora 3000. A new look-up table is simulated corresponding to a scattering wavelength of 525 nm. The datasets of PNSD and BC that were used are the same as those for producing the look-up table shown in Fig. 6a. During the Gucheng campaign, the variations in

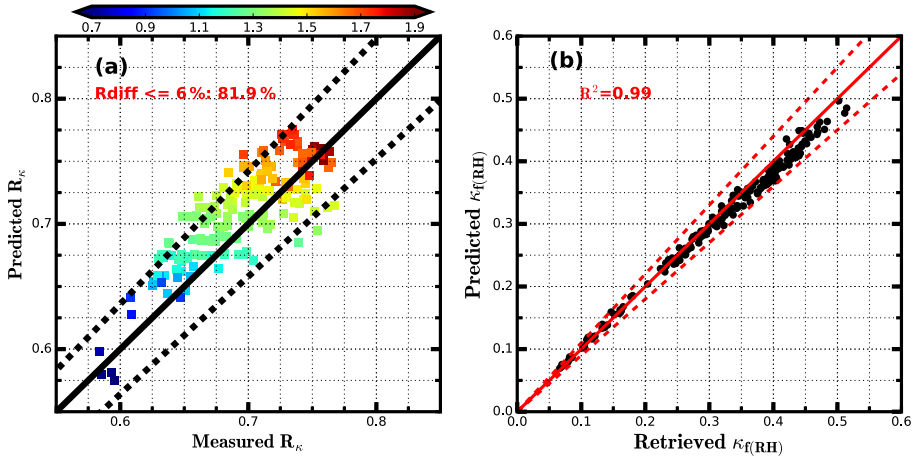

Figure 7. (a) The comparison between measured and predicted R_κ values. Colors represent values of Ångström exponents, texts with red color show the percentile of points with a relative difference (Rdiff) less than 6 %, and the two dashed lines are 6 % relative difference lines. **(b)** The comparison between $\kappa_{f(RH)}$ retrieved from Method 1 and predicted $\kappa_{f(RH)}$ using the new method introduced in Sect. 4.3. R^2 is the square of the correlation coefficient; the two dashed lines are 10 % relative difference lines.

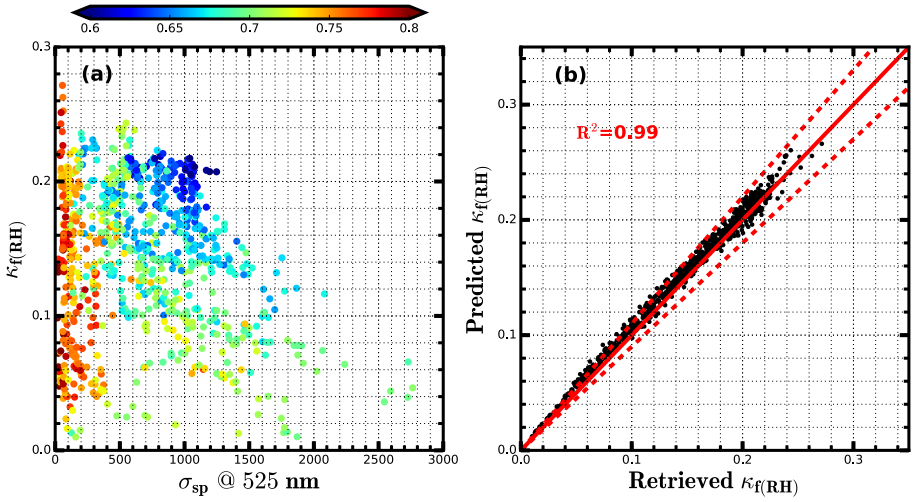

Figure 8. (a) The x axis represents σ_{sp} at 525 nm (M m^{-1}), the y axis represents retrieved $\kappa_{f(RH)}$, and colors of scatter points represent corresponding values of R_κ. **(b)** The comparison between $\kappa_{f(RH)}$ retrieved from Method 1 and predicted $\kappa_{f(RH)}$ using the new method. R^2 is the square of the correlation coefficient; the two dashed red lines represent 10 % deviations from the 1 : 1 line.

$\kappa_{f(RH)}$ and corresponding R_k with σ_{sp} at 525 nm are shown in Fig. 8a. Values of $\kappa_{f(RH)}$ range from 0.01 to 0.27, with an average of 0.14. During this campaign, $\kappa_{f(RH)}$ is relatively lower when σ_{sp} is high. Values of R_k range from 0.60 to 0.84, with an average of 0.7. Results of the comparison between $\kappa_{f(RH)}$ derived from Method 1 and Method 4 are shown in Fig. 8b. The results demonstrate that good consistency is achieved between $\kappa_{f(RH)}$ derived from Method 1 and Method 4. The square of correlation coefficient between them is 0.99.

The verification results of Method 4 using measurements from the Wangdu and Gucheng campaigns demonstrate that a good estimation of $\kappa_{f(RH)}$ can be achieved by only using measurements from a humidified nephelometer system. The processes of simulating the look-up table are independent of the size-resolved κ distribution, and the PNSDs that were used are from four different field campaigns that were conducted at different sites and in different seasons of the NCP. The verification datasets from two different field campaigns are totally independent of the look-up table and also from different sites and seasons of the NCP. These results demonstrate that the newly proposed method is applicable at different sites and in different seasons of the NCP. The results shown in Fig. 6b demonstrate that if the Ångström exponent and κ_{sca} are fixed, then R_k varies little. The maximum κ_{sca} of the look-up table is 0.4. If R_k is 0.8 (close

to the highest simulated R_k shown in Fig. 5b), the corresponding $f(\mathrm{RH}=80\,\%)$ is 2.6. According to the review of Titos et al. (2016), most $f(\mathrm{RH}=80\,\%)$ values for continental aerosols are lower than 2.6. The Ångström exponent range of the look-up table is 0.4 to 2.0. This demonstrates that the look-up table shown in Fig. 6a already covers large variation ranges of the Ångström exponent and κ_{sca} and can be used under different conditions. Thus, the newly proposed method of deriving $\kappa_{f(\mathrm{RH})}$ might also be applicable in other regions around the world. However, it should be pointed out that the look-up table shown in Fig. 6a is from simulations of measured continental aerosols without influences of desert dust, and it might not be suitable for estimating $\kappa_{f(\mathrm{RH})}$ when sea salt or dust particles prevail. In summary, this approach allows researchers to directly derive aerosol hygroscopicity from measurements of $f(\mathrm{RH})$ without any additional information about PNSD and BC, which is quite convenient for researchers to conduct aerosol hygroscopicity researches with measurements from a humidified nephelometer system.

5 Conclusions

In this paper, values of aerosol hygroscopicity parameter κ during the Wangdu campaign are first derived from measurements of $f(\mathrm{RH})$ by combining measurements of BC and PNSD in a dry state. The results show that during this field campaign, aerosol hygroscopicity varies a lot, and $\kappa_{f(\mathrm{RH})}$ ranges from 0.06 to 0.51, with an average of 0.34. Retrieved $\kappa_{f(\mathrm{RH})}$ values are further compared with κ_{250}, which is derived from measurements of HH-TDMA and good consistency is achieved.

Relationships between $\kappa_{f(\mathrm{RH})}$ and $f(\mathrm{RH})$ fitting parameters γ and κ_{sca} are further investigated in Sect. 4.2, which is the first time this has been done to our knowledge. A good linear relationship is found between $\kappa_{f(\mathrm{RH})}$ and κ_{sca} during the Wangdu campaign. Results of detailed analysis of the relationship between $\kappa_{f(\mathrm{RH})}$ and κ_{sca} demonstrate that the relationship between $\kappa_{f(\mathrm{RH})}$ and κ_{sca} is complicated, and the ratio $\kappa_{\mathrm{sca}}/\kappa_{f(\mathrm{RH})}$ (R_κ) varies a lot (0.5 to 0.84, with an average of 0.69).

In Sect. 4.3, a look-up table based on the Ångström exponent and κ_{sca} is developed to estimate R_κ. With this look-up table, R_κ as well as $\kappa_{f(\mathrm{RH})}$ can be directly estimated from measurements of a humidified nephelometer system. This method is further verified with measurements from two different campaigns. The verification results demonstrate that a quite good estimation of $\kappa_{f(\mathrm{RH})}$ can be achieved by only using measurements from a humidified nephelometer system, and this method is applicable at different sites and in different seasons of the NCP and might also be applicable in other regions around the world. This newly proposed approach allows researchers to estimate $\kappa_{f(\mathrm{RH})}$ without any additional information about PNSD and BC. This new finding directly links κ and $f(\mathrm{RH})$ and will make the humidified nephelometer system more convenient when it comes to aerosol hygroscopicity research. Finally, findings in this research may facilitate the intercomparison of aerosol hygroscopicity derived from different techniques, help parameterize $f(\mathrm{RH})$, and predict CCN properties with optical measurements.

Data availability. The data used are listed in the references and a repository at http://pan.baidu.com/s/1c2Nzc5a.

The Supplement related to this article is available online at https://doi.org/10.5194/acp-17-6651-2017-supplement.

Competing interests. The authors declare that they have no conflict of interest.

Acknowledgements. This work is supported by the National Natural Science Foundation of China (41590872, 41375134).

Edited by: B. Ervens
Reviewed by: three anonymous referees

References

Anderson, T. L. and Ogren, J. A.: Determining aerosol radiative properties using the TSI 3563 integrating nephelometer, Aerosol Sci. Tech., 29, 57–69, https://doi.org/10.1080/02786829808965551, 1998.

Bian, Y. X., Zhao, C. S., Ma, N., Chen, J., and Xu, W. Y.: A study of aerosol liquid water content based on hygroscopicity measurements at high relative humidity in the North China Plain, Atmos. Chem. Phys., 14, 6417–6426, https://doi.org/10.5194/acp-14-6417-2014, 2014.

Birmili, W., Stratmann, F., and Wiedensohler, A.: Design of a DMA-based size spectrometer for a large particle size range and stable operation, J. Aerosol Sci., 30, 549–553, https://doi.org/10.1016/s0021-8502(98)00047-0, 1999.

Boucher, O., Randall, D., Artaxo, P., Bretherton, C., Feingold, G., Forster, P., Kerminen, V.-M., Kondo, Y., Liao, H., Lohmann, U., Rasch, P., Satheesh, S. K., Sherwood, S., Stevens, B., and Zhang, X. Y.: Clouds and Aerosols, in: Climate Change 2013: The Physical Science Basis. Contribution of Working Group I to the Fifth Assessment Report of the Intergovernmental Panel on Climate Change, edited by: Stocker, T. F., Qin, D., Plattner, G.-K., Tignor, M., Allen, S. K., Boschung, J., Nauels, A., Xia, Y., Bex, V., and Midgley, P. M., Cambridge University Press, Cambridge, United Kingdom and New York, NY, USA, 571–658, 2013.

Brock, C. A., Wagner, N. L., Anderson, B. E., Attwood, A. R., Beyersdorf, A., Campuzano-Jost, P., Carlton, A. G., Day, D. A., Diskin, G. S., Gordon, T. D., Jimenez, J. L., Lack, D. A., Liao, J., Markovic, M. Z., Middlebrook, A. M., Ng, N. L., Perring, A. E., Richardson, M. S., Schwarz, J. P., Washenfelder, R. A., Welti, A., Xu, L., Ziemba, L. D., and Murphy, D. M.: Aerosol optical properties in the southeastern United States in summer

– Part 1: Hygroscopic growth, Atmos. Chem. Phys., 16, 4987–5007, https://doi.org/10.5194/acp-16-4987-2016, 2016.

Chen, J., Zhao, C. S., Ma, N., and Yan, P.: Aerosol hygroscopicity parameter derived from the light scattering enhancement factor measurements in the North China Plain, Atmos. Chem. Phys., 14, 8105–8118, https://doi.org/10.5194/acp-14-8105-2014, 2014.

Drinovec, L., Mocnik, G., Zotter, P., Prévôt, A. S. H., Ruckstuhl, C., Coz, E., Rupakheti, M., Sciare, J., Müller, T., Wiedensohler, A., and Hansen, A. D. A.: The "dual-spot" Aethalometer: an improved measurement of aerosol black carbon with real-time loading compensation, Atmos. Meas. Tech., 8, 1965–1979, https://doi.org/10.5194/amt-8-1965-2015, 2015.

Ervens, B., Cubison, M. J., Andrews, E., Feingold, G., Ogren, J. A., Jimenez, J. L., Quinn, P. K., Bates, T. S., Wang, J., Zhang, Q., Coe, H., Flynn, M., and Allan, J. D.: CCN predictions using simplified assumptions of organic aerosol composition and mixing state: a synthesis from six different locations, Atmos. Chem. Phys., 10, 4795–4807, https://doi.org/10.5194/acp-10-4795-2010, 2010.

Gunthe, S. S., King, S. M., Rose, D., Chen, Q., Roldin, P., Farmer, D. K., Jimenez, J. L., Artaxo, P., Andreae, M. O., Martin, S. T., and Pöschl, U.: Cloud condensation nuclei in pristine tropical rainforest air of Amazonia: size-resolved measurements and modeling of atmospheric aerosol composition and CCN activity, Atmos. Chem. Phys., 9, 7551–7575, https://doi.org/10.5194/acp-9-7551-2009, 2009.

Hennig, T., Massling, A., Brechtel, F. J., and Wiedensohler, A.: A tandem DMA for highly temperature-stabilized hygroscopic particle growth measurements between 90 % and 98 % relative humidity, J. Aerosol Sci., 36, 1210–1223, https://doi.org/10.1016/j.jaerosci.2005.01.005, 2005.

Kuang, Y., Zhao, C. S., Tao, J. C., and Ma, N.: Diurnal variations of aerosol optical properties in the North China Plain and their influences on the estimates of direct aerosol radiative effect, Atmos. Chem. Phys., 15, 5761–5772, https://doi.org/10.5194/acp-15-5761-2015, 2015.

Kuang, Y., Zhao, C. S., Ma, N., Liu, H. J., Bian, Y. X., Tao, J. C., and Hu, M.: Deliquescent phenomena of ambient aerosols on the North China Plain, Geophys. Res. Lett., 43, 8744–8750, https://doi.org/10.1002/2016GL070273, 2016a.

Kuang, Y., Zhao, C. S., Tao, J. C., Bian, Y. X., and Ma, N.: Impact of aerosol hygroscopic growth on the direct aerosol radiative effect in summer on North China Plain, Atmos. Environ., 147, 224–233, https://doi.org/10.1016/j.atmosenv.2016.10.013, 2016b.

Liu, H. J., Zhao, C. S., Nekat, B., Ma, N., Wiedensohler, A., van Pinxteren, D., Spindler, G., Müller, K., and Herrmann, H.: Aerosol hygroscopicity derived from size-segregated chemical composition and its parameterization in the North China Plain, Atmos. Chem. Phys., 14, 2525–2539, https://doi.org/10.5194/acp-14-2525-2014, 2014.

Liu, P. F., Zhao, C. S., Göbel, T., Hallbauer, E., Nowak, A., Ran, L., Xu, W. Y., Deng, Z. Z., Ma, N., Mildenberger, K., Henning, S., Stratmann, F., and Wiedensohler, A.: Hygroscopic properties of aerosol particles at high relative humidity and their diurnal variations in the North China Plain, Atmos. Chem. Phys., 11, 3479–3494, https://doi.org/10.5194/acp-11-3479-2011, 2011.

Ma, N., Zhao, C. S., Müller, T., Cheng, Y. F., Liu, P. F., Deng, Z. Z., Xu, W. Y., Ran, L., Nekat, B., van Pinxteren, D., Gnauk, T., Müller, K., Herrmann, H., Yan, P., Zhou, X. J., and Wiedensohler, A.: A new method to determine the mixing state of light absorbing carbonaceous using the measured aerosol optical properties and number size distributions, Atmos. Chem. Phys., 12, 2381–2397, https://doi.org/10.5194/acp-12-2381-2012, 2012.

Müller, T., Laborde, M., Kassell, G., and Wiedensohler, A.: Design and performance of a three-wavelength LED-based total scatter and backscatter integrating nephelometer, Atmos. Meas. Tech., 4, 1291–1303, https://doi.org/10.5194/amt-4-1291-2011, 2011.

Petters, M. D. and Kreidenweis, S. M.: A single parameter representation of hygroscopic growth and cloud condensation nucleus activity, Atmos. Chem. Phys., 7, 1961–1971, https://doi.org/10.5194/acp-7-1961-2007, 2007.

Pinnick, R. G., Jennings, S. G., and Chýlek, P.: Relationships between extinction, absorption, backscattering, and mass content of sulfuric acid aerosols, J. Geophys. Res.-Oceans, 85, 4059–4066, https://doi.org/10.1029/JC085iC07p04059, 1980.

Seinfeld, J. H. and Pandis, S. N.: Atmospheric chemistry and physics: from air pollution to climate change, John Wiley & Sons, 2006.

Tao, J. C., Zhao, C. S., Ma, N., and Liu, P. F.: The impact of aerosol hygroscopic growth on the single-scattering albedo and its application on the NO_2 photolysis rate coefficient, Atmos. Chem. Phys., 14, 12055–12067, https://doi.org/10.5194/acp-14-12055-2014, 2014.

Titos, G., Cazorla, A., Zieger, P., Andrews, E., Lyamani, H., Granados-Muñoz, M. J., Olmo, F. J., and Alados-Arboledas, L.: Effect of hygroscopic growth on the aerosol light-scattering coefficient: A review of measurements, techniques and error sources, Atmos. Environ., 141, 494–507, https://doi.org/10.1016/j.atmosenv.2016.07.021, 2016.

Wex, H., Neususs, C., Wendisch, M., Stratmann, F., Koziar, C., Keil, A., Wiedensohler, A., and Ebert, M.: Particle scattering, backscattering, and absorption coefficients: An in situ closure and sensitivity study, J. Geophys. Res.-Atmos., 107, 8122, https://doi.org/10.1029/2000jd000234, 2002.

Wu, Z. J., Zheng, J., Shang, D. J., Du, Z. F., Wu, Y. S., Zeng, L. M., Wiedensohler, A., and Hu, M.: Particle hygroscopicity and its link to chemical composition in the urban atmosphere of Beijing, China, during summertime, Atmos. Chem. Phys., 16, 1123–1138, https://doi.org/10.5194/acp-16-1123-2016, 2016.

You, Y., Smith, M. L., Song, M., Martin, S. T., and Bertram, A. K.: Liquid–liquid phase separation in atmospherically relevant particles consisting of organic species and inorganic salts, Int. Rev. Phys. Chem., 33, 43–77, https://doi.org/10.1080/0144235X.2014.890786, 2014.

Zhao, C., Tie, X., and Lin, Y.: A possible positive feedback of reduction of precipitation and increase in aerosols over eastern central China, Geophys. Res. Lett., 33, L11814, https://doi.org/10.1029/2006GL025959, 2006.

Zieger, P., Fierz-Schmidhauser, R., Weingartner, E., and Baltensperger, U.: Effects of relative humidity on aerosol light scattering: results from different European sites, Atmos. Chem. Phys., 13, 10609–10631, https://doi.org/10.5194/acp-13-10609-2013, 2013.